*Materials Transactions*, Vol. 45, No. 7 (2004) pp. 2062 to 2067
Special Issue on Grain Boundaries, Interfaces, Defects and Localized Quantum Structures in Ceramics


# Valence of Highly Dispersed Cerium Oxide Species on Silica Quantitatively Estimated by Ce $L_{III}$-edge XANES

Hisao Yoshida[1], Leny Yuliati[2,*], Tomoyo Hamajima[2*] and Tadashi Hattori[2]

[1]*Research Center for Advanced Waste and Emission Management (ResCWE), Nagoya University, Nagoya 464-8603, Japan*
[2]*Department of Applied Chemistry, Graduate School of Engineering, Nagoya University, Nagoya 464-8603, Japan*

A series of silica-supported cerium oxide samples having various cerium content were prepared by conventional impregnation method, followed by calcination in air. Ce $L_{III}$-edge XANES study revealed that highly dispersed cerium oxide species on silica surface were predominantly in trivalent oxidation state and cerium oxide nano-particles on silica contain mainly tetravalent cation like as $CeO_2$ bulk oxide. This elucidated that UV absorption band at 265 nm is assignable to Ce(III) species dispersed on silica.

(Received February 3, 2004; Accepted March 15, 2004)

***Keywords:*** *Cerium $L_{III}$-edge X-ray Absorption Near Edge Structure, silica-supported cerium oxide, valence, Ultraviolet absorption, highly dispersed cerium oxide species on silica*

## 1. Introduction

$SiO_2$-$CeO_2$ system such as Ce-containing glass has been known as for optical and photonics materials.[1,2] Cerium oxide has a high chemical reactivity with silica to make Si-O-Ce bond, which was also well studied in the field for polishing mechanism of $SiO_2$ with $CeO_2$.[3,4] Usually $CeO_2$ consists of Ce(IV) species with a minor portion of Ce(III). In $SiO_2$ matrix, Ce atom is believed to exist substitutionally as Ce(IV) or Ce(III) cation, and the ratio of these species varies with the Ce concentration and preparation method.[1,5–7]

These Ce species should show each photoabsorption band. However, the assignments have not been precisely determined; there are some variations in literature. This would be originated from the fact that UV absorption band of Ce species in silica system are much influenced by the structure or circumstance of Ce species. A band at 265 nm on the spectra of silica-supported $CeO_2$ (1 mass%) evacuated at 1073 K was assigned to charge transfer from oxygen to low coordinated Ce(III) and a band at 280 nm for the same sample before the treatment was assigned to charge transfer from oxygen to low coordinated Ce(IV).[5] On the other hand, in Ce-containing silica glass, it was claimed that Ce(III) exhibits absorption band around 320 nm due to the 4f-5d transition, while Ce(IV) exhibits one at shorter wavelength around 260–265 nm due to the electron transfer from ligand oxygen to Ce.[1,6,7] In another silica-supported $CeO_2$ system, the absorption band was observed at 280 nm on samples of low Ce content such as 1 mass%, and at 320 nm on samples of high Ce content such as 8 mass%.[8] Very unique spectra were also reported on silica-supported $CeO_2$ system of very low content such as 220 ppm, which were composed of several narrow bands in the 250–350 nm range.[8] In this way, although we could know the variation of Ce oxide species from the UV absorption spectra, the assignment seems not to have been well established on $SiO_2$-$CeO_2$ system. In addition, since the UV absorption coefficient for each species is probably much different from each other and it can easily vary with their environments,[9] quantitative estimation of these species by UV spectroscopy would be difficult.

Ce $L_{III}$-edge XANES spectroscopy has been proposed as a useful method for the quantitative determination of the ratio of Ce(III) and Ce(IV), since both species exhibit each distinguishable absorption peaks.[10–22] In the present study, a series of $SiO_2$-$CeO_2$ samples were prepared by impregnation method followed by calcination in air and studied by Ce $L_{III}$-edge XANES through a curve fitting analysis in order to know the ratio of Ce(III) and Ce(IV) and assignment of the UV absorption band for these species on silica.

## 2. Experimental

### 2.1 Materials

Amorphous silica ($SiO_2$, powder) was prepared from $Si(OEt)_4$ by sol-gel method followed by calcination in a flow of air at 773 K for 5 h.[23] BET surface area was $6.6 \times 10^2$ $m^2/g$. Silica-supported cerium oxide samples, $Ce/SiO_2$, were prepared by an impregnation method; calcined silica (1 g) was impregnated by aqueous solutions of $Ce(NO_3)_3$ (20 mL), and heated to dryness. Thus, the obtained powder was dried at 383 K for 12 h in an oven and calcined at 773 K in a flow of air for 5 h. The Ce content ($x$ mol%) was defined as $x = N_{Ce}(\mathrm{mol})/(N_{Ce}(\mathrm{mol}) + N_{Si}(\mathrm{mol})) \times 100$ and referred as to $Ce/SiO_2(x)$. Unsupported $CeO_2$ sample was commercially obtained and calcined in air at 773 K for 5 h. Other chemical reagents such as $Ce(NO_3)_3$, $Ce_2(SO_4)_3$, $Ce(SO_4)_2$, $Ce(OH)_4$ were employed as reference compounds for XANES spectra.

### 2.2 Measurements

Specific BET surface area was calculated from the amount of $N_2$ adsorption at 77 K. Powder X-ray diffraction (XRD) patterns were recorded on a Rigaku diffractometer RINT 1200 using Ni-filtered Cu-K$\alpha$ radiation (40 kV, 20 mA). Diffuse reflectance UV-vis spectra were recorded at room temperature on a JASCO V-570 equipped with an integrating sphere covered with $BaSO_4$. Before recording a UV-vis spectrum, the sample was heated in air up to 773 K, and then evacuated. Subsequently, the sample was treated with 13 kPa of oxygen at 773 K for 1 h, followed by evacuation at 773 K for 1 h. Thus, the sample was transferred to the optical cell

*Graduate Student, Nagoya University

without exposure to atmosphere by using a specially designed *in-situ* cell.

Most of Ce $L_{III}$-edge XANES spectra were mainly obtained at BL-9A station[24,25] of Photon Factory, Institute of Materials Structure Science, High Energy Accelerator Research Organization in Tsukuba (KEK-PF, Japan), with ring energy of 2.5 GeV and stored current of 300–450 mA. The spectra were recorded with a Si(111) double-crystal monochromator in a transmission mode or a fluorescence mode at room temperature. High energy X-rays from high order reflections were removed by a pair of flat quartz mirrors coated with Ni. The energy was defined by assigning the first characteristic peak of the Cu foil spectrum to 8978.9 eV.[26] The spectrum of the $Ce/SiO_2$ sample of high Ce loading (>1 mol%) was recorded in a transmission mode. For determination of incident x-ray intensity, an ionization chamber (17 cm) filled with $N_2$(30%)-He(70%) was used, and for transmission x-ray an ionization chamber (31 cm) filled with $N_2$(85%)-Ar(15%) was used. As for the sample of low Ce loading (<1 mol%), the fluorescence mode was employed by using the Lytle-detector[27] for fluorescent x-rays, whose ionization chamber (30 mm) was filled with Ar(100%), by using a Z-1 filter of Ti ($\mu t = 6$). The sample was pretreated at 773 K with 8 kPa $O_2$ for 1 h followed by evacuation for 1 h, and sealed with a polyethylene film in dry atmosphere. Some of samples was recorded at BL-7C station[28] of KEK-PF with a Si(111) double-crystal monochromator in the similar method to the above.

### 2.3 XANES analysis

Normalized XANES spectrum to the height of the edge jump was obtained through removal of contribution from absorption other than the $L_{III}$-edge absorption by the Ce atom.[29] The curve fitting analysis of XANES spectra was carried out by using arctangent $T(x)$ and Lorentzian $L(x)$ functions (eqs. 1–3):[30–37]

$$F(x) = T(x) + \sum_n L_n(x) \tag{1}$$

$$\begin{aligned} T(x) &= T_3(x) + T_4(x) \\ &= h \cdot \left(\frac{1}{2} + \frac{1}{\pi}\tan^{-1}\frac{(x - E_3)}{B}\right) \\ &\quad + (1 - h) \cdot \left(\frac{1}{2} + \frac{1}{\pi}\tan^{-1}\frac{(x - E_4)}{B}\right) \end{aligned} \tag{2}$$

$$L_n(x) = \frac{h_n}{1 + [(x - E_n)/d_n]^2} \tag{3}$$

where $F(x)$ = calculated XANES, $x$ = x-ray energy (eV), $h$ = maximum intensity, $E_3$, $E_4$, $E_n$ = energy position of each edge or peak (eV), $B$ = constant (eV), $d$ = half width at half maximum (eV).

Arctangent curve shows the transitions from Ce $2p_{3/2}$ to the continuum, while the Lorentzian curve represents transitions to unoccupied orbital or resonance. In order to estimate the ratio of Ce(III) to Ce(IV) quantitatively, we assumed that the spectra would be contributed from only Ce(III) and Ce(IV) species and the spectrum due to each species would be expressed by the sum of one arctangent curve and at least one Lorentzian curve (eq. 2). Using this assumption, the fraction of the arctangent curve (the "height" of arctangent) for Ce(III) will give us information about the relative ratio of Ce(III) to all Ce atoms in the sample.

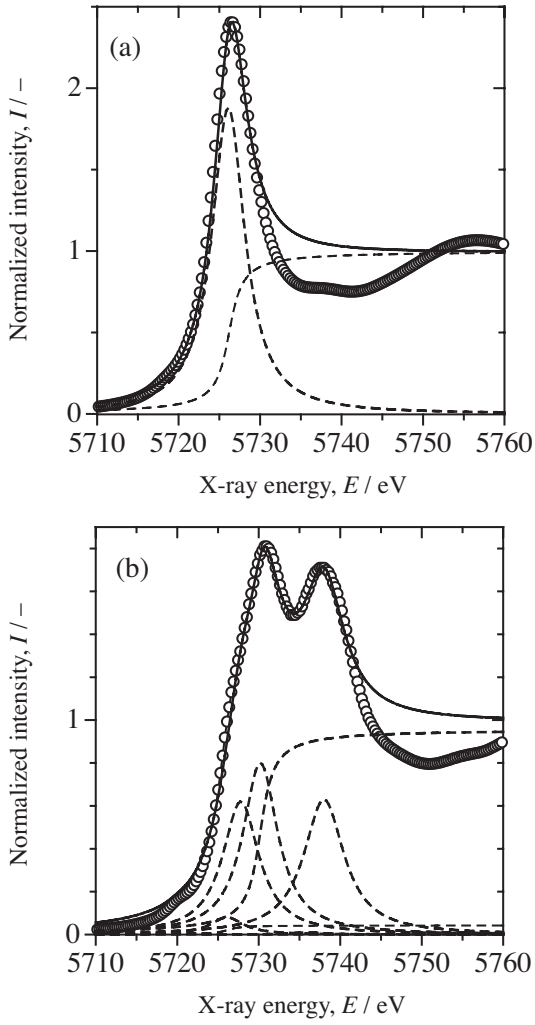


Fig. 1 Ce $L_{III}$-edge XANES spectra (simbols) of $Ce(NO_3)_3$ (a) and $CeO_2$ (b) and simulated spectra (solid lines), which are composed of some Lorentzian combined with arctangent functions (broken lines, see text and Table 1).

In the present fitting analysis, $Ce(NO_3)_3$ was used as a reference compound for Ce(III) and $CeO_2$ was used for Ce(IV). Figure 1 shows the XANES spectra of these two compounds with the best fitting results. The values of fitting parameters are listed in Table 1. The spectra was composed by six Lorentzian curves, called A, $B_0$, $B_1$, $B_2$, $C_1$, and $C_2$ following literature labeling[10] in addition to two arctangent curves, $T_3$ and $T_4$. It has been reported that $B_0$ is assigned to a $Ce^{3+}$ species, and the other peaks due to $Ce^{4+}$ species. In fitting analysis, all of spectra could be simulated using the set of parameters listed in Table 1. Although unsatisfied part remained for pre-edge region (5710-5720 eV for Ce(IV) in Fig. 1(b)) and post edge region (above 5730 eV for Ce(III), 5742 eV for Ce(IV)), the best fitting was judged on the main features of the target spectrum "by inspection" as suggested in literature.[30]

As for $Ce(NO_3)_3$, the spectrum seems simply to consist of one arctangent and one large Lorentzian, where the threshold

Table 1 Parameters of curve-fitting peaks with arctangent and Lorentzian functions in XANES spectra.

| Parameter | Sample | Arctangent[a] | | Lorentzian[b] | | | | | |
|---|---|---|---|---|---|---|---|---|---|
| | | $T_3$ | $T_4$ | A | $B_0$ | $B_1$ | $B_2$ | $C_1$ | $C_2$ |
| position, $E$/eV | | 5726.1 | 5730.2 | 5720.2 | 5726.1 | 5727.8 | 5730.2 | 5736.0 | 5738.1 |
| $B$ | | 1.2 | 1.2 | — | — | — | — | — | — |
| width, $d$/eV | | — | — | 1.84 | 2.47 | 2.71 | 2.60[c] | 2.58 | 3.00 |
| height, $h$/— | $Ce(NO_3)_3$ | 1.00 | 0.00 | 0.00 | 1.87 | 0.00 | 0.00 | 0.00 | 0.00 |
| | $CeO_2$ | 0.048 | 0.952 | 0.02 | 0.09 | 0.60 | 0.81 | 0.02 | 0.62 |
| | $Ce/SiO_2(0.01)$ | 0.738 | 0.262 | 0.02 | 1.38 | 0.35 | 0.10 | 0.04 | 0.30 |
| | $Ce/SiO_2(0.1)$ | 0.348 | 0.652 | 0.08 | 0.65 | 0.92 | 0.34 | 0.27 | 0.48 |
| | $Ce/SiO_2(2)$[d] | 0.132 | 0.868 | 0.01 | 0.31 | 0.64 | 0.81 | 0.28 | 0.74 |
| | $Ce/SiO_2(20)$ | 0.096 | 0.904 | 0.02 | 0.18 | 0.50 | 0.99 | 0.13 | 0.75 |

[a]For the name of the curves, see text and Fig. 1. $T_3$ corresponds to Ce(III) and $T_4$ corresponds Ce(IV).
[b]The small peak A for Ce(IV) was assigned to transition from $2p_{3/2}$ to 4f, which appear due to hybridization of 5d-4f orbitals though this transition is forbidden from the selection rule.[12–14] Peak $B_0$ is assigned to a Ce(III) species, which is due to transition to Ce $[2p^5(4f^1)5d^1]$ O $2p^6$ final state.[10,12–15] Peak $B_1$ and $B_2$ are due to transition to Ce $[2p^5(4f^1\ L)5d^{*1}]$ O $2p^5$ final state where an electron is transferred from ligand (L) orbitals, that is 2p of oxygen, to 4f shell of Ce, and due to transition to Ce $[(4f^2\ L)5d^{*1}]$ O $2p^4$ final state where two electrons are transferred from 2p of oxygen to 4f shell of Ce[10,15–17] Another suggestion for peaks $B_1$ and $B_2$ is splitting due to crystal-field effect.[14] Peak C corresponds to the transition to $2p^5(4f^0)5d^1$ final state,[10,12,13,15] where the splitting to $C_1$ and $C_2$ would be due to the crystal-field effect.[10,15] Another suggestion for peak $C_2$ is transition to Ce$[2p^5(4f^2)5d^1]$ O $2p^4$ final state.[17]
[c]The width for $B_2$ was 2.8 for $Ce/SiO_2(2)$ and $Ce/SiO_2(20)$.
[d]The spectrum of $Ce/SiO_2(2)$ was recorded at BL-7C station. Since the height of $B_0$ for $Ce(NO_3)_3$ recorded at this station was 2.34 and the height of $B_2$ for $CeO_2$ was 1.01 (these were different from the values for them in Table 1), the ratio of Ce(III) on $Ce/SiO_2(2)$ was determined by using these values.

($E_3$, 5726.1 eV) of arctangent for Ce(III), $T_3$, conformed to the maximum energy position of Lorentzian for $B_0$ peak that is main clear feature of this spectrum. From this fitting result, the energy positions of the functions for Ce(III) was fixed to 5726.1 eV and the ratio of the peak height of these two functions was also fixed to 1.87 during the fitting analysis for samples. $Ce_2(SO_4)_3$, which was another Ce(III) compound, showed quite similar XANES spectrum (Fig. 2), confirming the determined values on the position of the functions and the relative height of them (Table 1) should be available for the fitting analysis.

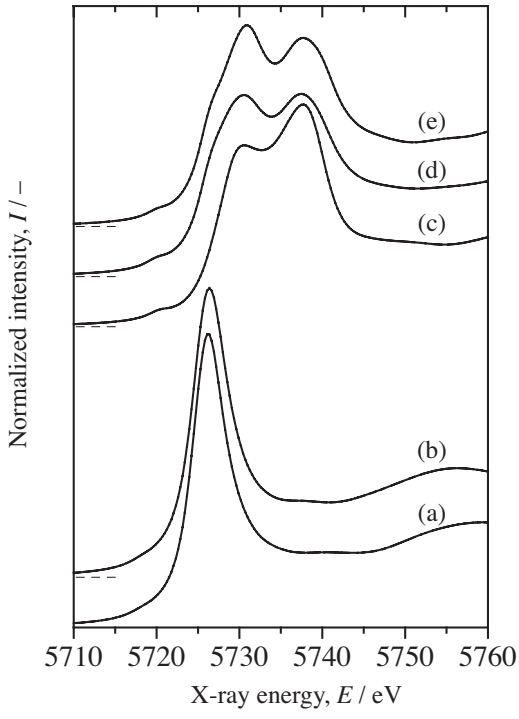


Fig. 2 Normalized Ce $L_{III}$-edge XANES of the reference Ce compounds; (a) $Ce_2(SO_4)_3$ and (b) $Ce(NO_3)_3$ are of Ce(III), (c) $Ce(SO_4)_2$, (d) $Ce(OH)_4$ and (e) $CeO_2$ are of Ce(IV).

The XANES spectrum of $CeO_2$ was a little complex, which was expressed by one arctangent $T_4$ and three major Lorentzians ($B_1$, $B_2$ and $C_2$) with minor three components (A, $B_0$ and $C_1$). Since major peaks were different from that for Ce(III) species, the threshold of $T_4$ was assumed to be the same as that for $B_2$, corresponding to the maximum of the spectra, 5730.2 eV. This assumption means that the threshold for continuum of Ce(III) and Ce(IV) was different from each other. The similar shift due to valence has been observed for rare earth.[31–34] The relative height of $B_2$ to $T_4$ was determined to be 0.85 (Table 1) for $CeO_2$.

During the fitting analysis for the prepared samples, the width of Lorentzian was fixed for each curve. Although the relative ratio of height among Lorentzian functions ($B_1$, $B_2$ and C) and their relative height to $T_4$ were preferably treated to be constant, the best fitting showed some variation. As shown in Fig. 2, the contribution of these peaks were not constant among three reference compounds; *i.e.*, $Ce(OH)_4$ and $Ce(SO_4)_2$ exhibited different distribution on B and C peaks from that for $CeO_2$ although they exhibited similarly assignable peaks in common.

The XANES spectrum of $CeO_2$ showed a minor shoulder ($B_0$) at the energy position of Ce(III) species, which is mentioned as Ce(III) impurities in literature.[10,11] During the fitting analysis of $CeO_2$ spectrum, the shoulder can not be discarded and it is treated as Ce(III) in this work because it was the same energy position as that of Ce(III). It can be considered that $CeO_2$ is an insulating mixed valence or interatomic intermediate-valence system having a mixture of multielectrons configurations $4f^0$ and $4f^1$ in the ground state.[12,13] But it does not close any other possibilities that the $B_0$ peak might be formed due to a delocalization of 4f state[14] or a slight reduction of the oxide by the intense photon beam in experiment.[12]

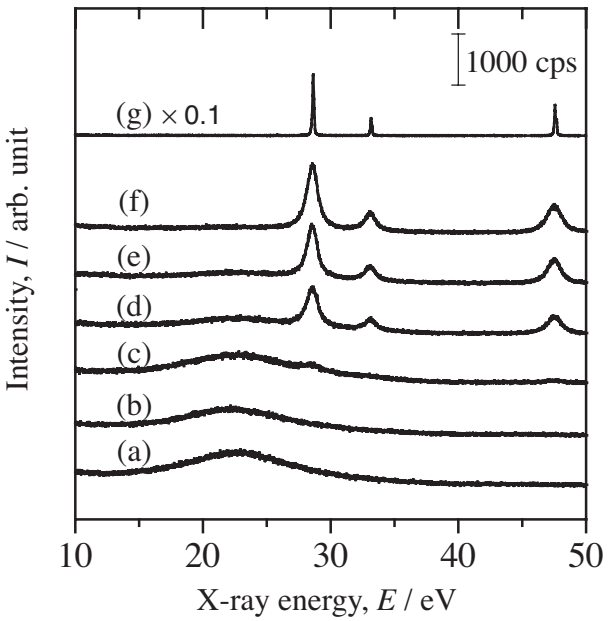


Fig. 3 X-ray diffraction patterns of (a) $SiO_2$, the $Ce/SiO_2$ samples containing (b) 0.1, (c) 2, (d) 4, (e) 8 and (f) 20 mol% of Ce, and (g) $CeO_2$.

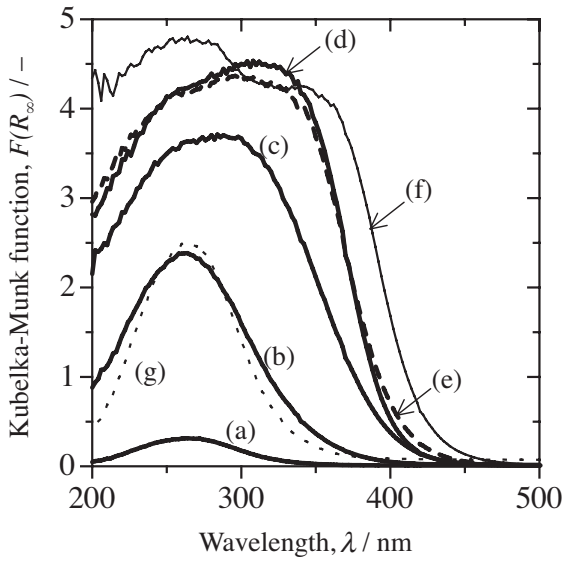


Fig. 4 Diffuse reflectance UV-visible absorption spectra of the $Ce/SiO_2$ samples containing (a) 0.01, (b) 0.1, (c) 2, (d) 4 and (e, broken line) 20 mol% of Ce, and (f, thin line) $CeO_2$. The spectrum (g, dotted line) was obtained from curve (a) multiplied by 8.

## 3. Results and Discussion

### 3.1 The structure of the $Ce/SiO_2$ samples

Figure 3 shows powder X-ray diffraction patterns of the samples. $SiO_2$ showed broad feature around 23 degrees (Fig. 3a) and $CeO_2$ showed clear three diffractions (Fig. 3g). The $Ce/SiO_2$ sample containing 0.1 mol% exhibited only the broad feature due to amorphous $SiO_2$ support and no diffractions due to $CeO_2$ (Fig. 3b). The sample of 2 mol% Ce showed very small diffractions due to $CeO_2$ over amorphous feature due to $SiO_2$ (Fig. 3c). The $Ce/SiO_2$ containing over 4 mol% exhibited the diffractions due to $CeO_2$ crystallites (Figs. 3d–f), indicating these samples have $CeO_2$ particles on silica support. The diffraction intensity of $Ce/SiO_2(2)$ (Fig. 3c) is much less than that of $Ce/SiO_2(4)$ (Fig. 3d), indicating the particle on the former would have smaller particle size and/or less crystallinity than the latter. The halo diffraction due to silica amorphous phase of $Ce/SiO_2(4)$ was smaller than $Ce/SiO_2(2)$, suggesting that the amorphous structure also would be changed when the cerium species aggregated and $CeO_2$ crystallites were formed.

Figure 4 shows diffuse reflectance UV-visible spectra of the $Ce/SiO_2$ samples and bulk $CeO_2$. The bulk $CeO_2$, which is semiconductor, showed a large absorption band less than 420 nm (Fig. 4f), which corresponds to the band gap transition from valence band to conduction band. The $Ce/SiO_2$ sample containing 20 and 4 mol% exhibited also a large band (Figs. 4d and e), where the absorption edge seemed to be shifted to shorter wavelength probably as results of due to quantum size effect,[38,39] suggesting that Ce on silica existed as $CeO_2$ particles and their sizes would be smaller than unsupported bulk $CeO_2$. In general, the quantum size effect is observed on the semiconductor particle of less than ca. 10 nm. Thus, the $CeO_2$ particles on silica in $Ce/SiO_2$ of large content around 4-20 mol% would be nano-sized $CeO_2$ particles.

The $Ce/SiO_2$ containing less than 0.1 mol% showed a small and narrow band at 265 nm probably due to a certain transition (Figs. 4a and b). Similar result has been reported on literature and variously assigned as mentioned above. The $Ce/SiO_2(2)$ sample showed a complex band with shoulders at 265 nm and 300 nm (Fig. 4c). This spectrum and XRD (Fig. 3c) implied that there were at least two kinds of Ce species, one was for low content sample and another was high content sample.

The results from XRD patterns and UV-vis spectra suggested that $Ce/SiO_2$ sample of lower content such as 0.1 and 0.01 mol% would dominantly have highly dispersed Ce oxide species exhibiting an absorption band at 265 nm and $Ce/SiO_2$ sample of higher content than 4 mol% would have mainly $CeO_2$ nano-sized particles exhibiting large and broad absorption band.

### 3.2 Valence of Ce species

Figure 5 shows normalized XANES spectra of the $Ce/SiO_2$ samples and reference compounds. As mentioned above, the reference compound for Ce(III), $Ce(NO_3)_3$, showed a large "white line" absorption, $B_0$ peak at 5726.1 eV (Fig. 5h), while the reference of Ce(IV), $CeO_2$, showed a complex spectra having two peaks above edge, $B_2$ and $C_2$ (Fig. 5g). The $Ce/SiO_2$ samples also showed these peaks. The samples containing smaller amount of Ce showed $B_0$ peak dominantly with C peak as minor, while the samples of high content exhibited similar spectra to that of $CeO_2$. The spectra of the samples could not be composed by the linear combination of only the two reference spectra of $Ce(NO_3)_3$ and $CeO_2$. This means that Ce $L_{III}$-edge XANES contains information about not only valence but also local structure, and the local structure certainly varied with the loading amount of Ce on silica surface. The highly dispersed Ce oxide species would have different local structure from the bulk $CeO_2$ as suggested from UV spectra.[8]

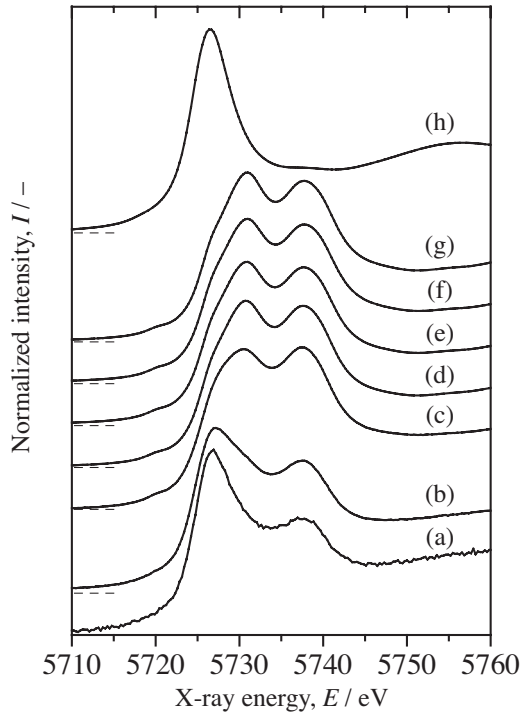


Fig. 5 Normalized Ce $L_{III}$-edge XANES of the $Ce/SiO_2$ samples containing (a) 0.01, (b) 0.1, (c) 2, (d) 4, (e) 8 and (f) 20 mol% of Ce, with reference compounds (g) $CeO_2$ and (h) $Ce(NO_3)_3$.

As a whole, however, the series of spectra implies that the XANES spectra were predominantly influenced by the valence of Ce. Thus, in order to get more quantitative information about valence of Ce, we carried out the fitting analysis in the manner described above. The best parameters for fitting are listed in Table 1. The ratio of Ce(III) on each sample corresponds to the value of $T_3$. It is obvious that every sample contains both Ce(III) and Ce(IV). The variation of the ratio of Ce(III) to all Ce atoms in the sample was plotted in Fig. 6, showing that the ratio of Ce(III) gradually decreased with an increase of Ce content. It was confirmed that Ce

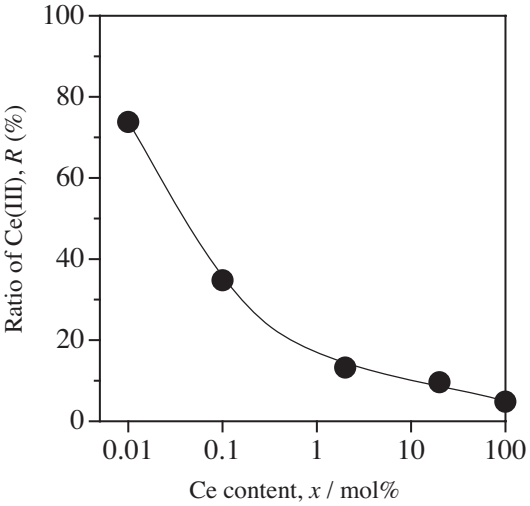


Fig. 6 The ratio of Ce(III) in the $Ce/SiO_2$ samples and $CeO_2$ determined by curve fitting analysis of Ce $L_{III}$-edge XANES versus Ce content.

cations in the highly dispersed Ce oxide species on silica has a tendency to become trivalent Ce(III) cations, while Ce cations in $CeO_2$ nano-particles mainly exist as tetravalent Ce(IV) cations.

### 3.3 UV absorption species on $Ce/SiO_2$

The UV absorption band of the $Ce/SiO_2$(*0.01*) sample seems closed to be symmetric (Fig. 4a), suggesting almost one kind species are there. Since the major species on this sample was elucidated to be Ce(III) oxide species, it is proposed that the absorption band at 265 nm is assignable to Ce(III) oxide species that would be highly dispersed on silica. The assignment of transition mechanism, whether it is charge transfer or 4f-5d transition, could not be clarified in the present study.

The fraction of Ce(III) in $Ce/SiO_2$(*0.01*) was estimated to be 74% from XANES analysis and that in $Ce/SiO_2$(*0.1*) was to be only 35%. The band intensities of these two samples were roughly in proportion to the amount of Ce(III) in the sample and the band shape seemed similar to each other (Figs. 4a and b). When the spectrum of $Ce/SiO_2$(*0.01*) (Fig. 4a) was multiplied by 8 (Fig. 4g), it was found that these curves were not exactly the same. This suggests that the fraction of Ce(IV) species dispersed on silica also show a broad absorption band less than ca. 400 nm to some extent though they exhibited lower coefficient for UV absorption than the Ce(III) species.

On the other hand, Ce(IV) species as major species in $CeO_2$ nano-particles dispersed on silica would exhibit similar absorption to that of the bulk $CeO_2$ (Figs. 4d and e).

The $Ce/SiO_2$(*2*) sample having Ce(III) of 13% showed two shoulders at 265 nm and 300 nm (Fig. 4c) and their intensities were almost the same. The former at 265 nm would be assignable to Ce(III), which was 13%, and the latter at 300 nm would be assignable to Ce(IV) in $CeO_2$ nano-particle, which was 87%. This again confirms that the former has much higher absorption coefficient.

## 4. Conclusion

UV spectra and the fitting analysis of Ce $L_{III}$-edge XANES spectra of silica-supported Ce oxide revealed the followings:

(1) the ratio of Ce(III) gradually increased with a decrease of Ce content, in other words, Ce cation in the highly dispersed Ce oxide species on silica has a tendency to be trivalent Ce(III) cation,

(2) highly dispersed Ce(III) oxide species on silica would have different local structure from the bulk $CeO_2$,

(3) the highly dispersed Ce(III) oxide species on silica exhibited photoabsorption band at 265 nm with relatively high coefficient, while dispersed Ce(IV) oxide species exhibited broad absorption bands with low atomic coefficient.

## Acknowledgements

The X-ray absorption experiment at the Ce $L_{III}$-edge was performed under the approval of the Photon Factory Program Advisory Committee (Proposal No. 2003G248). This work was partially supported by a Grant-in-Aid for Scientific

Research on Priority Areas (417 and 751) from the Ministry of Education, Culture, Sports, Science and Technology (MEXT) of the Japanese Government.

## REFERENCES


1) G. E. Malashkevich, E. N. Poddenezhny, I. M. Melnichenko and A. A. Boiko: J. Non-Cryst. Solids **188** (1995) 107–117.
2) T. Tulun and H. Akinci: Ceramics Intern. **23** (1997) 141–148.
3) L. M. Cook: J. Non-Cryst. Solids **120** (1990) 152–171.
4) T. Hoshino, Y. Kurata, Y. Terasaki and K. Susa: J. Non-Cryst. Solids **283** (2001) 129–136.
5) A. Bensalem, J. C. Muller and F. Bozon-Verduraz: J. Chem. Soc., Faraday Trans. **88** (1992) 153–154.
6) A. Patra, G. De, D. Kundu and D. Ganguli: Mater. Lett. **42** (2000) 200–206.
7) R. Reisfeld and C. K. Jorgensen: *Laser and excited states of rare-earths*, ed. by R. Reifeld and C. K. Jorgensen, (Springer-Verlag, 1997).
8) A. Bensalem, F. Bozon-Verduraz, M. Delamar and G. Bugli: Appl. Catal. A **121** (1995) 81–93.
9) M. A. Sainz, A. Durán and J. M. Fernández Navarro: J. Non-cryst. Solids **121** (1990) 315–318.
10) J. El Fallah, S. Boujana, H. Dexpert, A. Kiennemann, J. Majerus, O. Touret, F. Villain and F. Le Normand: J. Phys. Chem. **98** (1994) 5522–5533.
11) P. Nachimuthu, W.-C. Shih, R.-S. Liu, L.-Y. Jang and J.-M. Chen: J. Solid State Chem. **149** (2000) 408–413.
12) L. Douillard, M. Gautier, N. Thromat, M. Henriot, M. J. Guittet, J. P. Duraud and G. Tourillon: Phys. Rev. B. **49** (1994) 16171–16180.
13) A. Bianconi, A. Marcelli, H. Dexpert, R. Karnatak, A. Kotani, T. Jo and J. Petiau: Phys. Rev. B **35** (1987) 806–812.
14) H. Dexpert, R. C. Karnatak, J.-M. Esteva, J. P. Connerade, M. Gasgnier, P. E. Caro and L. Albert: Phys. Rev. B. **36** (1987) 1750–1753.
15) Y. Takahashi, H. Shimizu, H. Kagi, H. Yoshida, A. Usui and M. Nomura: Earth and Planetary Sci. Lett. **182** (2000) 201–207.
16) Y. Takahashi, H. Shimizu, A. Usui, H. Kagi and M. Nomura: Geochim. Cosmochim. Acta **64** (2000) 2929–2935.
17) A. Trovarelli: Ed., *Catalysis by ceria and related materials*, (Imperial College Press, 2002) pp. 201.
18) F. Le Normand, L. Hilaire, K. Kili, G. Krill and G. Maire: J. Phys. Chem. **92** (1988) 2561–2568.
19) A. Bianconi, A. Marcelli, M. Tomellini and I. Davoli: J. Magn. Magn. Mater. **47** (1985) 209–211.
20) A. Kotani, T. Jo and J. C. Parlebas: Adv. Phys. **37** (1988) 37–85.
21) J. G. Darab, H. Li and J. D. Vienna: J. Non-Cryst. Solids **226** (1998) 162–174.
22) Z. Wu, J. Zhang, R. E. Benfield, Y. Ding, D. Grandjean, Z. Zhang and X. Ju: J. Phys. Chem. B **106** (2002) 4569–4577.
23) H. Yoshida, C. Murata and T. Hattori: J. Catal. **194** (2000) 364–372.
24) M. Nomura and A. Koyama: J. Synchrotron Rad. **6** (1999) 182–184.
25) M. Nomura and A. Koyama: Nucl. Instr. Meth. Phys. Res. A **467–468** (2001) 733–736.
26) T. Yoshida, T. Tanaka, H. Yoshida, T. Funabiki and S. Yoshida: J. Phys. Chem. **100** (1996) 2302–2309.
27) F. W. Lytle, R. B. Greegor, D. R. Sandstrom, E. C. Marques, J. Wong, C. L. Spiro, G. P. Huffman and F. E. Huggins: Nucl. Instr. Meth. Phys. Res. A **226** (1984) 542–548.
28) M. Nomura, A. Koyama and M. Sakurai: KEK Report **91-1** (1991) 1–30.
29) T. Tanaka, H. Yamashita, R. Tsuchitani, T. Funabiki and S. Yoshida: J. Chem. Soc., Faraday Trans. 1 **84** (1988) 2987–2999.
30) S. Yoshida and T. Tanaka: *X-ray absorption fine structure for catalysts and surfaces*, ed by Y. Iwasawa (World Scientific Publishing, Singapore, 1996) pp. 304–325.
31) T. Tanaka, T. Hanada, S. Yoshida, T. Baba and Y. Ono: Jpn. J. Appl. Phys. **32** (1993) Suppl. 32-2, 481–483.
32) T. Baba, S. Hikita, R. Koide, Y. Ono, T. Hanada, T. Tanaka and S. Yoshida: J. Chem. Soc. Faraday Trans. **89** (1993) 3177–3180.
33) T. Yoshida, T. Tanaka, S. Yoshida, H. Handa, S. Hikita, T. Baba and Y. Ono: J. Physique IV 7, Colloque C2 (1997) 915–916.
34) T. Yoshida, T. Tanaka, S. Yoshida, S. Hikita, T. Baba and Y. Ono: Solid State Commun. **114** (2000) 255–259.
35) K. Nishi, K. Shimizu, M. Takamatsu, H. Yoshida, A. Satsuma, T. Tanaka, S. Yoshida and T. Hattori: J. Phys. Chem. B **102** (1998) 10190–10195.
36) K. Shimizu, Y. Kato, T. Yoshida, H. Yoshida, A. Satsuma and T. Hattori: Chem. Commun. **1999**, 1681–1682.
37) Y. Kato, K. Shimizu, N. Matsushita, T. Yoshida, H. Yoshida, A. Satsuma and T. Hattori: Phys. Chem. Chem. Phys. **3** (2001) 1925–1929.
38) L. Brus: J. Phys. Chem. **90** (1986) 2555–2560, and references therein.
39) M. R. Hoffmann, S. T. Martin, W. Choi and D. W. Bahnemann: Chem. Rev. **95** (1995) 69–96.